PCCP

Check for updates

Understanding photochemical pathways of laser-induced metal ion reduction through byproduct analysis†

Laysa M. Frias Batista, Michael Moody, Chamari Weththasingha, Ella Kaplan [ID], Irtiza Faruque, M. Samy El-Shall [ID] * and Katharine Moore Tibbetts [ID] *

Laser-induced reduction of metal ions is attracting increasing attention as a sustainable route to ligand-free metal nanoparticles. In this work, we investigate the photochemical reactions involved in reduction of Ag^+ and $[AuCl_4]^-$ upon interaction with lasers with nanosecond and femtosecond pulse duration, using strong-field ionization mass spectrometry and spectroscopic assays to identify stable molecular byproducts. Whereas Ag^+ in aqueous isopropyl alcohol (IPA) is reduced through plasma-mediated mechanisms upon femtosecond laser excitation, low-fluence nanosecond laser excitation induces electron transfer from IPA to Ag^+. Both nanosecond and femtosecond laser excitation of aqueous $[AuCl_4]^-$ produce reactive chlorine species by Au–Cl bond homolysis. Formation of numerous volatile products by IPA decomposition during both femtosecond and nanosecond laser excitation of $[AuCl_4]^-$ is attributed to enhanced optical breakdown by the Au nanoparticle products of $[AuCl_4]^-$ reduction. These mechanistic insights can inform the design of laser synthesis procedures to improve control over metal nanoparticle properties and enhance byproduct yields.
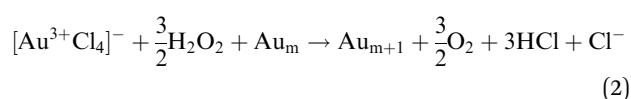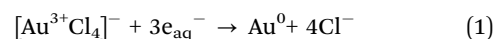
1. Introduction

Photochemical reduction of metal salts has been explored for decades as a sustainable method to produce metal nanoparticles without toxic chemical reducing agents.[1–6] Light sources from the infrared through γ-ray spectral regions initiate distinct chemical reaction pathways that reduce metal ions.[1] Ionizing radiation directly dissociates solvent molecules to provide strong reducing agents such as solvated electrons and organic radicals.[2,3] Ultraviolet (UV) photons reduce metal ions through electronic excitation of a photosensitizer to produce organic radicals or direct excitation and dissociation of metal ion complexes.[4,5] Intense pulsed lasers initiate reaction pathways observed with both ionizing and UV radiation to reduce metal ions in what is called laser reduction in liquid (LRL).[6]
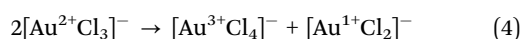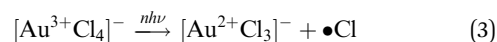
LRL typically involves focusing intense laser pulses into a liquid medium, which ionizes and dissociates solvent molecules to produce a localized plasma containing reactive chemical species that reduce metal ions. In aqueous solution, the primary reactive species are the same as those observed in radiolysis: hydrated electrons (e_{aq}^-), hydroxyl radicals ($OH^\bullet$), hydrogen

radicals ($H^\bullet$) and hydrogen peroxide (H_2O_2).[7–11] LRL has been widely used to produce Au nanoparticles (NPs) from aqueous solutions of the tetrachloroaurate complex $[AuCl_4]^-$[7–20] and Ag NPs from aqueous solutions of the salts $AgNO_3$ or $AgClO_4$.[21–26] For $[AuCl_4]^-$, Au^{3+} reduction is initiated by cleavage of an Au–Cl bond, whereas reduction of an Ag salt involves direct electron capture by free Ag^+ ions in solution.

Under LRL conditions that form plasma, hydrated electrons and H_2O_2 contribute to the reduction of $[AuCl_4]^-$ into Au atoms and clusters through the reactions[10]

$$[Au^{3+}Cl_4]^- + 3e_{aq}^- \rightarrow Au^0 + 4Cl^- \tag{1}$$

$$[Au^{3+}Cl_4]^- + \tfrac{3}{2}H_2O_2 + Au_m \rightarrow Au_{m+1} + \tfrac{3}{2}O_2 + 3HCl + Cl^- \tag{2}$$

We recently reported that LRL using 532 nm, 8 ns laser pulses at low fluences below the plasma formation threshold can also reduce $[AuCl_4]^-$ to Au NPs.[19] To account for the observed $[AuCl_4]^-$ reduction without the aid of reactive plasma species, we proposed that the reduction to Au atoms proceeds through direct photolysis of Au–Cl bonds by mechanisms that had previously been proposed for photochemical reduction by UV photons,[27,28]

$$[Au^{3+}Cl_4]^- \xrightarrow{nh\nu} [Au^{2+}Cl_3]^- + \bullet Cl \tag{3}$$

$$2[Au^{2+}Cl_3]^- \rightarrow [Au^{3+}Cl_4]^- + [Au^{1+}Cl_2]^- \tag{4}$$

Department of Chemistry, Virginia Commonwealth University, Richmond, VA 23284, USA. E-mail: mselshal@vcu.edu, kmtibbetts@vcu.edu

$$[Au^{1+}Cl_2]^- \xrightarrow{nh\nu} Au^0 + Cl^- + \bullet Cl \qquad (5)$$

Under low-fluence nanosecond LRL at 532 nm, reaction (3) was proposed to be initiated by laser-induced heating based on simulations showing that transient temperatures of 580 K, near the spinodal temperature of water, were sustained for about 100 µs after irradiation with a single 8 ns laser pulse.[19]

A recent report by Liu et al. confirmed that reaction (3) initiates UV photolysis of aqueous $[AuCl_4]^-$ through X-ray transient absorption spectroscopy measurements.[29] They found that excitation at 263 nm formed $[Au^{2+}Cl_3]^-$ within the instrument response function of 79 ps, indicating rapid Au–Cl bond homolysis following electronic excitation of $[AuCl_4]^-$. In contrast, upon excitation at 800 nm (the wavelength used in femtosecond LRL studies[7-20]), the $[Au^{2+}Cl_3]^-$ did not appear until 5 ns after the initial pulse. The authors surmised that this delayed Cl loss resulted from the time required for a hydrated electron to diffuse to an $[AuCl_4]^-$ molecule, indicating that the initial reduction step in LRL with near-infrared femtosecond lasers is

$$[Au^{3+}Cl_4]^- + e_{aq}^- \rightarrow [Au^{2+}Cl_3]^- + Cl^-, \qquad (6)$$
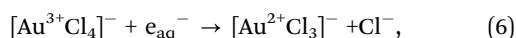
which is consistent with the general mechanism in reaction (1).

Whereas aqueous $[AuCl_4]^-$ can easily be reduced due to its labile Au–Cl bonds and high reduction potential (E^0 = +1.002 V for reaction (1)[30]), efficient photoreduction of Ag^+ typically requires an auxiliary polymer reducing agent,[31] photosensitizer,[32] or aliphatic alcohol.[33-35] LRL experiments with both nanosecond and femtosecond pulsed lasers indicate that reduction of aqueous Ag^+ to produce stable Ag NPs only occurs in the presence of a capping agent,[21-23] or a radical scavenger.[24-26] The requirement of a radical scavenger for Ag NP formation by LRL is attributed to the facile back-oxidation of Ag^0 atoms by $OH^\bullet$ radicals present in laser plasma.[24,25] LRL of Ag^+ with 355 nm nanosecond pulses at a fluence sufficient for two-photon ionization of water but not plasma generation was found to produce stable Ag NPs in the presence of surfactants.[22] However, it remains unknown whether two-photon excitation of Ag^+ in the presence of alcohols using visible wavelengths can initiate Ag^+ reduction at fluences below the plasma threshold.

To unravel the photochemical reaction pathways associated with $[AuCl_4]^-$ and Ag^+ reduction, we consider LRL under two different excitation conditions: high-density plasma from tightly focused femtosecond laser pulses and nonionizing low-fluence nanosecond laser excitation. For both conditions, we characterize stable molecular byproducts of metal ion reduction in water and aqueous solutions of isopropyl alcohol (IPA). Strong-field ionization mass spectrometry[36] is used to analyze the composition of the headspace gas after LRL because the more common method of gas chromatography-mass spectrometry (GC-MS)[37-40] is not suitable for aqueous solutions due to water-induced degradation of GC columns.[41] Combined with spectroscopic assays for oxidized byproducts, we both verify the pathways in reactions (1)–(5) and identify new pathways involving activation of IPA by metal ions and the metal nanoparticle products. These insights into metal ion reduction pathways can lead to better control of the properties of metal nanoparticles produced by LRL.

2. Experimental methods

2.1 Materials

Potassium tetrachloroaurate(III) (KAuCl_4, Strem Chemicals); silver perchlorate (AgClO_4), titanium dioxide (Sigma Aldrich); potassium permanganate, sodium acetate (Alfa Aesar); N,N-diethyl-p-phenylenediamine sulfate (DPD, ACROS Organics); sulfuric acid, hydrogen peroxide, sodium oxalate, potassium hydroxide, potassium chloride, isopropyl alcohol, and acetic acid (Fisher Scientific) were used as received.

2.2 Sample preparation

All solutions were prepared using Millipore Ultrapure water with resistivity 18.2 M Ω cm^{-1} at 25 °C as the solvent. All working solutions were freshly prepared before laser processing. The pH of working solutions containing metal ions was adjusted to 5.6 ± 0.3 with KOH. For headspace gas analysis, working solutions contained 1 mM KAuCl_4 or AgClO_4 in water or 100 mM aqueous IPA, along with solutions containing no metal ions as controls. For samples used in DPD and titanium sulfate assays, working solutions contained 0.1 mM aqueous $[AuCl_4]^-$. Samples of water were also irradiated as controls. The lower metal ion concentration for spectroscopic assays was used to ensure that absorbances of OD < 2.0 were obtained.

2.3 Laser processing

The experimental setups for processing with laser pulses of nanosecond[19] and femtosecond[10] duration have been described previously. Briefly, nanosecond laser processing was conducted with a Nd:YAG laser system (Lab 170–30, Spectra Physics) operated at the second harmonic, producing 532 nm, 8 ns, pulses at a 30 Hz repetition rate was set to a pulse energy of 100 mJ. A loosely focused geometry was used where laser beam was down-collimated to a diameter of 7 mm before interaction with the precursor solutions. Femtosecond laser processing was conducted using a commercial titanium-sapphire chirped-pulse amplifier (Astrella, Coherent, Inc., Santa Clara, CA, USA), delivering 30 fs pulses, with the bandwidth centered at 800 nm and a repetition rate of 1 kHz. A tight-focusing geometry with large numerical aperture producing a measured focal beam waist of approximately 6.5 µm[10] was used with pulse energy of 1 mJ, producing a peak intensity of approximately 2×10^{16} W cm^{-2} (ignoring losses). Experimental working solutions were processed with the nanosecond or femtosecond laser in 3 mL batches in a sealed cuvette for 60 minutes for headspace gas analysis. The cuvette containing the working solution was first evacuated so that the mass spectrum before laser processing could be measured (see Section 2.4).

2.4 Strong-field ionization mass spectrometry

Mass spectrometry (MS) of headspace gas was conducted using 1300 nm, 20 fs pulses for ionization as described previously.[36]

This journal is © the Owner Societies 2023

Phys. Chem. Chem. Phys., 2023, 25, 18844–18853 | 18845

Briefly, a portion of the 800 nm titanium-sapphire output was converted to 1300 nm in an optical parametric amplifier and focused to a peak intensity of 10^{14} W cm^{-2} into the extraction region of a linear time-of-flight mass spectrometer (Jordan TOF, Grass Valley, CA). A sealed quartz cuvette containing working solution was attached to the ultrahigh vacuum chamber (base pressure 3×10^{-9} Torr) and evacuated through a variable effusive leak valve. Once evacuated, the valve was adjusted to produce a working pressure of 3×10^{-7} torr consisting of headspace gases. Mass spectra were recorded by averaging over 100 000 laser shots using a 1 GHz digital oscilloscope (Wave-Runner 610Zi, Teledyne LeCroy). Mass spectra were normalized either to the area under the H_2O^+ ion signal at m/z 18 (for samples without IPA) or to IPA$^+$ peak at m/z 60 (for samples containing IPA).

2.5 Spectroscopic assays

Free chlorine species (Cl_2, ClOH, ClO$^-$) were detected using the standard assay based on N,N-diethyl-p-phenylenediamine (DPD).[42] Details of DPD oxidation by free chlorine from the initial dication, dpd^{2+}, to the semiquinoid radical, dpd^{2+}, are given in the ESI.† The dpd^{2+} exhibits strong absorbance at 551 nm that is used to quantify oxidizing species based on a calibration curve (ESI,† Fig. S1). Detection of H_2O_2 was performed using an adapted spectroscopic assay from ref. 43 based on the formation of pertitanic acid from titanium sulfate, $Ti(SO_4)_2$, and described in our previous work.[10] The absorbance of pertitanic acid at 407 nm was used to quantify H_2O_2 concentration based on a calibration curve (ESI,† Fig. S2).

The general procedure for both spectroscopic assays was as follows. 25 mM KCl was added to laser-processed samples to precipitate any Au NPs that were formed, then samples were centrifuged using a Fisher Scientific accuSpin Micro17 microcentrifuge for 30 min at 13 000 rpm. Following centrifugation, 2 mL of supernatant liquid was collected. All types of samples were processed following the above procedure (even those that produced no NPs) to eliminate any artifacts of sample processing. For DPD assay, acetate buffer (200 µL) was added to adjust the sample pH to ∼5. Then, DPD reagent (100 µL) was added right and the absorbance at 551 nm was measured using a commercial UV-vis spectrophotometer (Agilent 8453). For titanium sulfate assay, 400 µL of titanium(IV) sulfate (25 mM) was added to the cuvette and the absorbance of pertitanic acid at 407 nm measured.

3. Results and discussion

Chemical byproducts of laser-induced Ag$^+$ and [AuCl$_4$]$^-$ reduction were measured in two solutions that have been widely employed in LRL synthesis of Ag and Au NPs: metal ions in water[8–10,12–15,19–23] and in water/IPA.[11,17,18,21,26] MS analysis was performed on the headspace gas from working solutions in a sealed cuvette both before and after laser processing. The MS before laser processing was recorded to determine the species initially present so that any new products formed by laser

processing could easily be identified. To corroborate reaction pathways suggested by MS analysis, spectroscopic assays using DPD and titanium sulfate were conducted for selected reaction conditions. We first report the products and reaction pathways induced by laser processing of water and aqueous IPA in the absence of metal ions in Section 3.1. Analysis of additional reaction pathways activated by the presence of Ag$^+$ and [AuCl$_4$]$^-$ is then presented in Sections 3.2 and 3.3, respectively. A summary of reaction pathways and further discussion is provided in Section 3.4.

3.1 Laser-induced reactions in water and aqueous IPA

Femtosecond laser processing of water is known to produce H_2 and H_2O_2 from the optical breakdown plasma.[7,10,44,45] MS analysis of laser-processed water confirmed H_2 production using femtosecond laser pulses, but no H_2 was observed after nanosecond laser processing (ESI,† Fig. S3). H_2O_2 was detected by titanium sulfate assay only after femtosecond laser processing (ESI,† Fig. S4). These results indicate that ionization and decomposition of water does not occur for nanosecond laser processing under the low-fluence conditions used.

Fig. 1a shows a representative mass spectrum of 100 mM aqueous IPA before laser processing ('before', grey) and spectra of aqueous IPA after processing with the femtosecond laser ('fs', red) and nanosecond laser ('ns', green). The 'before' spectrum contains prominent peaks at m/z 60 (IPA parent ion), 45 (C_2H_5O fragment of IPA), 44 (C_2H_4O fragment of IPA), and 18 (H_2O). The IPA fragments at m/z 45 and 44 are also observed in electron impact mass spectra from the NIST spectral database.[46] Whereas processing with the nanosecond laser results in a spectrum with the same peaks as the 'before' spectrum, processing with the femtosecond laser produces four new peaks indicated by the black circles in Fig. 1a. To more easily visualize these spectral changes, the 'before' spectrum was subtracted off from the spectra after laser processing to produce the difference spectra shown in Fig. 1b. New species in the spectrum processed with the femtosecond laser (red) at m/z 2, 16, 42, 44, and 58 are assigned to H_2, CH_4, C_3H_6 (propene), C_2H_4O (acetaldehyde), and C_3H_6O (acetone). The peaks marked with a * are fragmentation products of acetone and propene.[46] Although m/z 44 was observed in the 'before' spectrum as an IPA fragmentation product, the positive difference peak after femtosecond processing (inset, Fig. 1b) suggests that a small amount of acetaldehyde was produced. In contrast, the m/z 44 feature after nanosecond laser processing contains negative and positive components due to slight shifts in the peak location between the spectra taken before and after laser processing. Peak shapes consisting of negative and positive components are observed in difference spectra for all species present in the 'before' spectrum due to this peak shifting (ESI,† Fig. S5 illustrates the shift of the m/z 45 peak).

The products H_2, CH_4, acetaldehyde, and acetone have been previously observed in γ radiolysis[47] and 185 nm UV photolysis[48] of IPA. It is expected that femtosecond laser processing of aqueous IPA would produce similar products as these previous studies because both irradiation methods produce solvated
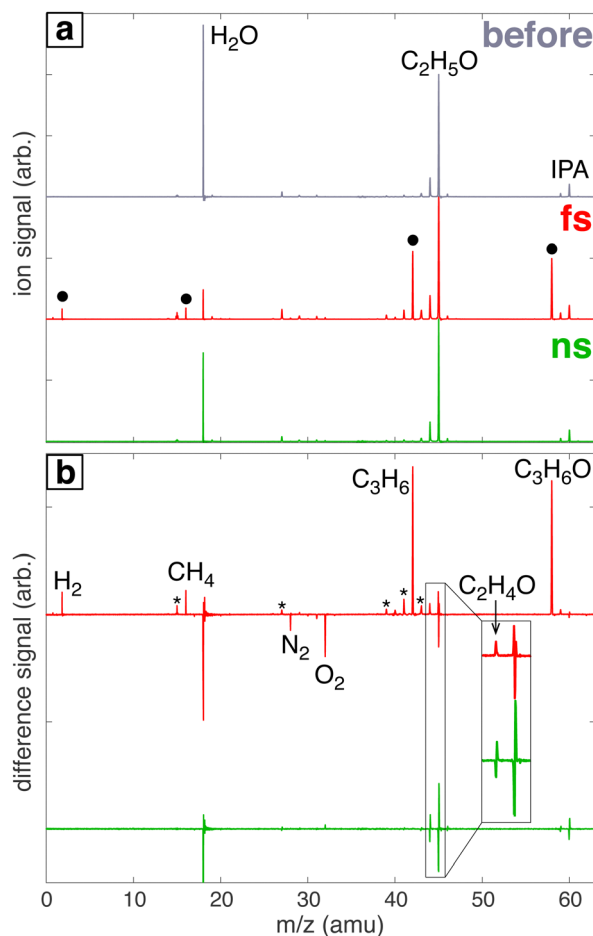
18846 | *Phys. Chem. Chem. Phys.*, 2023, **25**, 18844–18853

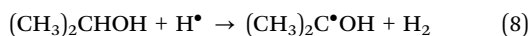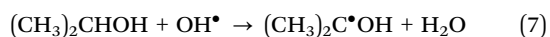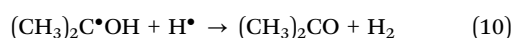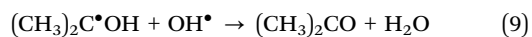This journal is © the Owner Societies 2023

Fig. 1 (a) Mass spectra of headspace gas samples of water/IPA solution before (grey) and after processing with femtosecond (red) or nanosecond (green) laser. (b) Difference mass spectra after laser processing with new species indicated. Peaks with a * denote fragmentation products of acetone and propene. The inset magnifies the region of m/z 44–45 to show the formation of C_2H_4O after femtosecond laser processing.

electrons, hydroxyl radicals (OH•), and hydrogen radicals (H•) in water.[2,6] In particular, the reactions that produce acetone during femtosecond laser processing are likely initiated by OH• or H• radicals according to the proposed reactions in γ radiolysis studies,[2]

$$(CH_3)_2CHOH + OH^\bullet \rightarrow (CH_3)_2C^\bullet OH + H_2O \quad (7)$$

$$(CH_3)_2CHOH + H^\bullet \rightarrow (CH_3)_2C^\bullet OH + H_2 \quad (8)$$

Abstraction of a hydrogen atom from the resulting ketyl radical, $(CH_3)_2C^\bullet OH$, with OH• or H• then produces acetone,

$$(CH_3)_2C^\bullet OH + OH^\bullet \rightarrow (CH_3)_2CO + H_2O \quad (9)$$

$$(CH_3)_2C^\bullet OH + H^\bullet \rightarrow (CH_3)_2CO + H_2 \quad (10)$$

In contrast to acetone, the formation of propene (m/z 42) during femtosecond laser processing is unexpected because both γ radiolysis and UV photolysis report <1% propene yield compared to H_2, CH_4, and acetone.[47,48] IPA can react with H• and OH• or 2H• to produce propene through the reactions

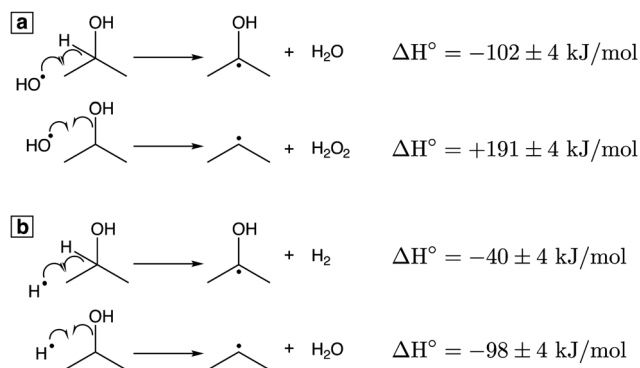
Fig. 2 Reactions of IPA with OH• (a) and H• (b) with ΔH° values at 298.15 K.[49]

$$(CH_3)_2CHOH + OH^\bullet + H^\bullet \rightarrow C_3H_6 + 2H_2O \quad (11)$$

$$(CH_3)_2CHOH + 2H^\bullet \rightarrow C_3H_6 + H_2 + H_2O \quad (12)$$
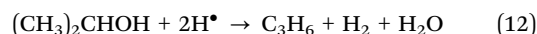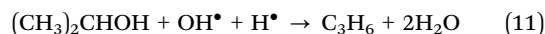
To understand the competition between acetone and propene formation, we consider the possible reactions of IPA with OH• (Fig. 2a) and H• (Fig. 2b). All thermochemical values are taken from ref. 49. Both OH• and H• can abstract the hydrogen on the carbon α to the OH group to produce the ketyl radical ($\Delta_f H^\circ = -96 \pm 4$ kJ mol^{-1}), which is the precursor to acetone formation (reactions (9) and (10)). Formation of propene requires cleavage of the C–O bond to produce the less stable isopropyl radical ($\Delta_f H^\circ = +89 \pm 4$ kJ mol^{-1}); abstraction of an additional H atom then forms propene. The highly exothermic abstraction of the α hydrogen by OH• ($\Delta H^\circ = -102 \pm 4$ kJ mol^{-1}, Fig. 2(a)) is consistent with radiolysis studies indicating that 89% of OH• reaction with IPA occurs by α hydrogen abstraction.[50] This favorable reaction enthalpy explains why acetone is a major product of IPA oxidation. In contrast, formation of the isopropyl radical by reaction with OH• is endothermic ($\Delta H^\circ = +191 \pm 4$ kJ mol^{-1}, Fig. 2a), but the same reaction with H• is exothermic ($\Delta H^\circ = -98 \pm 4$ kJ mol^{-1}, Fig. 2b). Because abstraction of the α hydrogen by H• is less exothermic ($\Delta H^\circ = -40 \pm 4$ kJ mol^{-1}, Fig. 2b) than C–O bond cleavage, the formation of propene likely proceeds through H• attack on IPA to produce the isopropyl radical, as previously proposed in gas-phase Ar plasma studies of IPA.[51]

The low propene yield in radiolysis despite an exothermic ΔH° for attack of H• on IPA to produce the isopropyl radical implies the existence of a high kinetic barrier to this reaction, likely due to the energy required to break the C–O bond. To rationalize the apparent ease of overcoming this barrier, we consider a key difference between femtosecond laser processing and γ radiolysis or UV photolysis. Specifically, focusing intense laser pulses in liquid media under optical breakdown conditions generates laser-driven shock waves that can reach transient pressures exceeding 1 GPa[52] and cavitation bubbles where gas-phase reactions can occur.[39] These conditions have been proposed to induce mechanical C–C bond formation reactions in liquid alkanes.[53] Hence, laser-induced shock waves can open up additional reaction pathways in femtosecond laser processing

This journal is © the Owner Societies 2023

Phys. Chem. Chem. Phys., 2023, **25**, 18844–18853 | **18847**

that are inaccessible in radiolysis. For propene formation from IPA, laser-induced shock waves could facilitate C–O bond cleavage through the reaction shown in Fig. 2b or overcome the modest endothermic barrier to direct dehydrogenation of IPA to propene[49]

$$C_3H_8O \rightarrow C_3H_6 + H_2O \quad \Delta H^\circ = 50 \pm 2 \text{ kJ mol}^{-1}$$
(13)
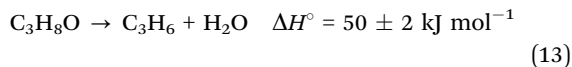
In either case, the high propene yield observed in Fig. 1 indicates femtosecond laser processing can overcome kinetic barriers present under radiolytic conditions.

The experiments in this section have established the baseline solvent reactions that occur in water and IPA/water solution under femtosecond laser processing and confirmed that no reactions occur under low-fluence nanosecond laser processing. With this knowledge, we turn to investigations of how added metal ions open up additional reaction pathways for both nanosecond and femtosecond laser processing.

3.2 Laser-induced reduction of Ag$^+$

LRL of Ag$^+$ in water does not produce stable Ag NPs.[21–26] Although Ag$^+$ is reduced by hydrated electrons at diffusion-limited rates[34] to produce Ag^0 atoms,

$$Ag^+ + e_{aq}^- \rightarrow Ag^0(aq)$$
(14)
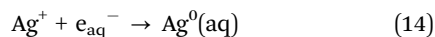
OH$^\bullet$ radicals in laser plasma rapidly back-oxidize Ag^0[24,25]

$$Ag^0 + OH^\bullet \rightarrow Ag^+ + OH^-$$
(15)
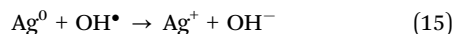
In femtosecond laser processing, no net reduction of Ag$^+$ was observed at concentrations below 300 mM.[23] Although nanosecond laser processing at sufficiently high fluence to ionize water can accomplish net reduction of Ag$^+$ to Ag^0, these studies reported unstable large Ag NPs that rapidly precipitated out of solution.[21,22] Consistent with these prior studies, we observed no Ag NP formation under nanosecond or femtosecond laser processing in water. MS analysis of the headspace gases found identical results as found for pure water: H$_2$ was produced during femtosecond laser processing and no new products were formed during nanosecond laser processing (ESI,† Fig. S6). Results from the titanium sulfate assay confirmed that Ag^0 is back-oxidized through reaction (15): the H$_2$O$_2$ yield in the presence of 0.1 mM Ag$^+$ was reduced by 50% compared to the yield obtained in pure water at the same femtosecond laser processing conditions (ESI,† Fig. S7).

Hydroxyl radical scavengers including ammonia[24,25] and IPA[26] suppress reaction (15), enabling production of Ag NPs by femtosecond LRL. In high-fluence nanosecond LRL, the addition of IPA was reported to lower the Ag$^+$ reduction rate by 25% due to its scavenging behavior.[21] MS analysis of the headspace gas was performed after laser processing of 1 mM Ag$^+$ in 100 mM aqueous IPA (raw spectra shown in ESI,† Fig. S8). The resulting difference spectra in Fig. 3 indicate that the same reaction products are formed as in femtosecond laser processing of aqueous IPA (*cf.*, Fig. 1), whereas only acetone is formed during nanosecond laser processing. Oxidation of IPA to acetone during nanosecond laser processing is accompanied by partial conversion of Ag$^+$ to Ag NPs, observed in the
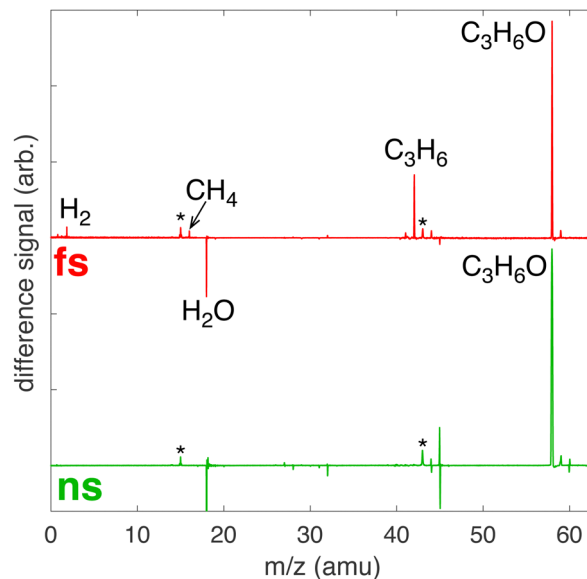

Fig. 3 Difference MS for femtosecond (red) and nanosecond (green) laser processing of 1 mM Ag$^+$ in 100 mM aqueous IPA with major products indicated. Peaks with a * denote fragmentation products of acetone.

absorbance spectrum of the laser-processed solution (ESI,† Fig. S9). These reactions do not appear to involve OH$^\bullet$ radicals because no H$_2$O$_2$ was detected from nanosecond laser processing (ESI,† Fig. S10).

The observed formation of acetone as a byproduct of Ag$^+$ reduction during nanosecond laser processing suggests that the reaction mechanism proceeds by electron transfer from an IPA molecule to Ag$^+$ within a solvent cage, as proposed by Hada *et al.* for Ag$^+$ reduction by 254 nm UV photolysis,[33]

$$Ag^+ + (CH_3)_2CHOH + H_2O \rightarrow Ag^0 + H_3O^+ + (CH_3)_2C^\bullet OH$$
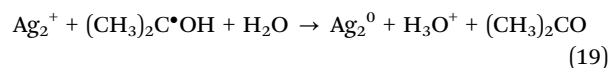(16)
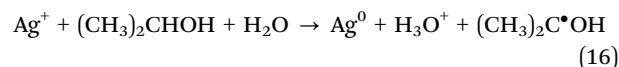
Reaction (16) produces a ketyl radical that can further be oxidized to acetone. Because no H$_2$O$_2$ was detected, it is unlikely that the ketyl radical oxidizes to acetone by OH$^\bullet$ *via* reaction (9). Instead, the ketyl radical can reduce an additional Ag$^+$ ion to produce acetone. It has been proposed that the ketyl radical directly reduces Ag$^+$ *via* electron transfer through the reaction[4,32,33]

$$Ag^+ + (CH_3)_2C^\bullet OH + H_2O \rightarrow Ag^0 + H_3O^+ + (CH_3)_2CO$$
(17)
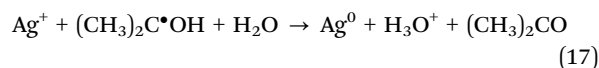
However, the standard oxidation potential $E^0 = +1.8$ V for the ketyl radical is not strong enough to reduce aqueous Ag$^+$ because $E^0 (Ag^+/Ag^0) = -1.8$ V according to Henglein *et al.*[34,35] Instead, they proposed that the ketyl radical reduces the Ag$_2^+$ cluster that rapidly forms from Ag^0 *via* the reaction

$$Ag^0 + Ag^+ \rightarrow Ag_2^+$$
(18)
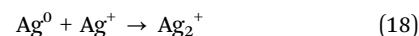
Because $E^0 (Ag_2^+/Ag_2) = -0.44$ V,[34] the reduction of Ag$_2^+$ by the ketyl radical to produce acetone

$$Ag_2^+ + (CH_3)_2C^\bullet OH + H_2O \rightarrow Ag_2^0 + H_3O^+ + (CH_3)_2CO$$
(19)

18848 | *Phys. Chem. Chem. Phys.*, 2023, **25**, 18844–18853

This journal is © the Owner Societies 2023

is thermodynamically favorable. Hence, we expect that reaction (19) produces the acetone observed in our experiments.

The photochemical reactions (16) through (19) were initiated by 254 nm (4.9 eV) photons in ref. 33. For the same reactions to occur with 532 nm (2.3 eV) photons from the nanosecond laser, absorption of two photons by the solvent cage containing Ag^+ and IPA must occur. The peak intensity of $\sim 3 \times 10^8$ W cm^{-2} in our experiments[19] is likely sufficient for 2-photon absorption. Nevertheless, our observation that Ag^+ reduction proceeds in the presence of IPA but not in pure water suggests that the energy required to initiate reaction (16) is lower than that required for electron transfer from a water molecule to Ag^+ in a solvent cage also proposed by Hada *et al.*[33]

$$Ag^+ + 2H_2O \rightarrow Ag^0 + H_3O^+ + OH^\bullet \qquad (20)$$
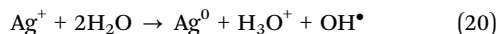
Because reaction (20) is initiated with 254 nm photons, we can conclude that the energy required for reaction (16) with IPA is likely less than 4.6 eV (two 532 nm photons) and the energy required for reaction (20) is above 4.6 eV but less than 4.9 eV.

In contrast to the electron transfer mechanism that produces only acetone as a byproduct for nanosecond laser excitation, femtosecond LRL of Ag^+ appears to proceed primarily by plasma-mediated reactions involving solvated electrons and IPA scavenging of $OH^\bullet$ as previously proposed[24,26] because no additional byproducts beyond those of IPA decomposition were observed in Fig. 3. We cannot rule out the participation of the electron-transfer mechanism in reactions (16) through (19) since higher quantities of acetone relative to other products are observed from femtosecond LRL in Fig. 3. However, experimental constraints preclude quantitative analysis of products using strong-field ionization mass spectrometry, so we cannot conclude that significantly more acetone is formed from IPA when Ag^+ is present.

3.3 Laser-induced reduction of $[AuCl_4]^-$

Whereas both femtosecond and nanosecond LRL require IPA for net reduction of Ag^+, $[AuCl_4]^-$ is easily converted to Au NPs in water.[7–10,13–15,18–20] MS analysis of 1 mM $[AuCl_4]^-$ in water (ESI,† Fig. S11) showed that H_2 was produced with femtosecond laser processing, as for pure water and aqueous Ag^+. No H_2 was formed by nanosecond laser processing. Neither condition produced Cl_2 or other volatile chlorine species that might be expected if $Cl^\bullet$ radicals are formed in the Au^{3+} reduction pathways described in reactions (3) through (5) in the Introduction. To determine whether $Cl^\bullet$ radicals are formed, we used the DPD assay (Section 2.5) to quantify the presence of stable free chlorine species ($ClOH$, ClO^-). The titanium sulfate assay was also performed for solutions subject to the same laser processing conditions to isolate the contributions of H_2O_2, which can oxidize DPD.[54] Laser processing was performed for 10 minutes with the femtosecond laser and 60 minutes with the nanosecond laser to ensure that 100% of the $[AuCl_4]^-$ was converted to Au NPs (ESI,† Fig. S12) because $[AuCl_4]^-$ also oxidizes DPD.

The quantified yields of pertitanic acid and dpd^{2+} after laser processing of water and 0.1 mM $[AuCl_4]^-$ are shown in Fig. 4. Tabulated yields can be found in the ESI,† Table S1. Pertitanic
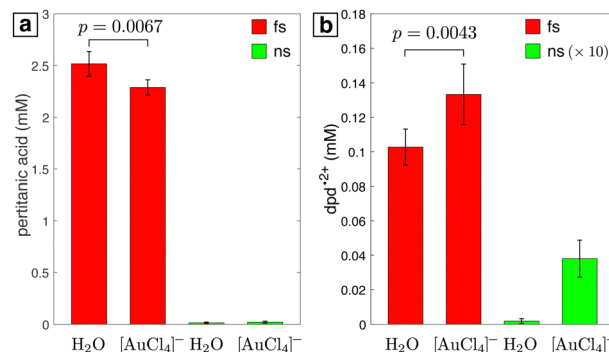

Fig. 4 Quantified yields of pertitanic acid (a) and dpd^{2+} (b) in samples of water and 0.1 mM $[AuCl_4]^-$ after processing with femtosecond (red) or nanosecond (green) laser. Values for the nanosecond laser in (b) are magnified by a factor of 10 for clarity. Brackets between the femtosecond samples indicate *p* values obtained from the two-tailed *t*-test.

acid is only observed upon femtosecond laser processing (Fig. 4a), with a 9% lower yield in 0.1 mM $[AuCl_4]^-$ than in water. The lower yield is due to H_2O_2 consumption through the autocatalytic reduction of $[AuCl_4]^-$ in the presence of Au NPs, as reported previously.[7,8,10] In contrast, the dpd^{2+} yield after femtosecond laser processing is 29% higher in $[AuCl_4]^-$ than in water (Fig. 4b). Because a decrease in dpd^{2+} yield in $[AuCl_4]^-$ would be expected if H_2O_2 were the only oxidant present, the statistically significant increase in dpd^{2+} ($p = 0.0043$ by two-tailed *t*-test performed in MATLAB) indicates presence of free chlorine species in addition to H_2O_2. The presence of oxidized dpd^{2+} after nanosecond laser processing of $[AuCl_4]^-$ (Fig. 4b) indicates that free chlorine species are generated under these conditions as well. Since no H_2O_2 is formed, this result confirms that direct Au–Cl bond homolysis drives $[AuCl_4]^-$ reduction in nanosecond laser processing, consistent with the mechanism proposed in our previous work.[19] The formation of free chlorine species during femtosecond laser processing is surprising because $[AuCl_4]^-$ reduction is widely thought to proceed by reaction with hydrated electrons instead of Au–Cl bond homolysis.[9–11] This issue will be further discussed in Section 3.4.

MS analysis of the volatile reaction products of $[AuCl_4]^-$ in IPA/water indicates that addition of Au substantially enhances the decomposition of IPA in both femtosecond and nanosecond laser processing. A plethora of new products are observed with both femtosecond and nanosecond laser processing in Fig. 5, enumerated in Table 1. The enhanced formation of chemical products from IPA decomposition likely arises from the presence of the Au NPs that are formed by LRL of $[AuCl_4]^-$.

Au NPs are known to enhance optical breakdown of water and alcohols during nanosecond laser processing.[37–39] Low-fluence nanosecond laser processing of IPA and Au NPs was reported to produce acetone, acetaldehyde, and methanol as major products.[38] In another study, nanosecond laser ablation of an Au target in ethylene glycol was found to produce H_2, CH_4, and CO as major products.[39] The nanosecond sample shows no clear evidence of acetaldehyde due to the peak shape at *m/z* 44 and we cannot conclude whether methanol and CO formed due to contamination from O_2 at *m/z* 32 and N_2 at *m/z* 28.

This journal is © the Owner Societies 2023

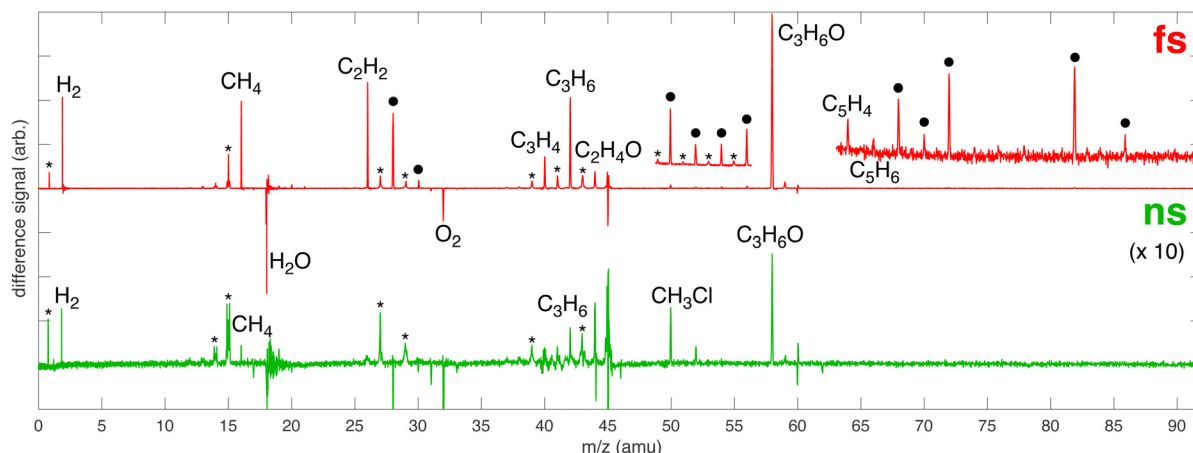*Phys. Chem. Chem. Phys.*, 2023, **25**, 18844–18853 | 18849

Fig. 5 Difference MS for femtosecond (red) and nanosecond (green) laser processing of 1 mM $[AuCl_4]^-$ in 100 mM aqueous IPA with major products indicated. The ● denotes that multiple species can contribute to the peak and the * indicates a peak due to fragmentation. The nanosecond spectrum is magnified by a factor of 10 to clearly show all products. Insets magnify the regions m/z 49–57 and 63–91 in the femtosecond spectrum to show low-yield products.

Table 1 Peak assignments for new species in Fig. 5 based on data from NIST Standard Reference Database 69.[46] The 'x' denotes the presence of the species

m/z	Assignment	fs	ns
2	H_2	x^a	x
16	CH_4	x^a	x
26	C_2H_2	x	
28	C_2H_4, CO	x	
30	C_2H_6, CH_2O	x	
40	C_3H_4	x	
42	C_3H_6	x^a	x
44	C_2H_4O	x^a	
50	CH_3 ^{35}Cl, C_4H_2	x	x
52	CH_3 ^{37}Cl, C_4H_4	x	x
54	C_4H_6, C_3H_2O	x	
56	C_4H_8, C_3H_4O	x	
58	C_3H_6O	x^a	x^a
64	C_5H_4	x	
66	C_5H_6	x	
68	C_5H_8, C_4H_4O	x	
70	C_5H_{10}, C_4H_6O	x	
72	C_5H_{12}, C_4H_8O, $C_3H_4O_2$	x	
82	C_6H_{10}, C_5H_6O	x	
86	C_6H_{14}, $C_5H_{10}O$, $C_4H_6O_2$	x	

^{a} Also observed with added Ag^+ (Fig. 3).

Nevertheless, the formation of acetone, CH_4, and H_2 supports the assertion that the Au NPs formed by LRL of $[AuCl_4]^-$ facilitate optical breakdown under low-fluence nanosecond laser processing because neither CH_4 nor H_2 were observed in Fig. 1 or 3.

Femtosecond laser excitation at 800 nm is known to efficiently form and excite plasma in the vicinity of Au NPs.[55] The resulting enhancement of the laser-induced shock waves can facilitate C–C coupling reactions, as proposed previously.[53] The MS peaks in the range of m/z 64–86 in Fig. 5 contain four or more carbon atoms (Table 1), suggesting that enhanced plasma reactivity imparted by the Au NPs induces C–C bond formation in our experiments. Excess plasma energy imparted by Au NPs
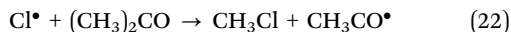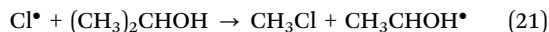
can also account for the formation of the alkynes C_2H_2 (m/z 26), C_3H_4 (m/z 40), C_4H_2 (m/z 50), and C_5H_4 (m/z 64). The alkynes acetylene (C_2H_2, $\Delta H_f^\circ = 54.6 \pm 0.1$ kJ mol^{-1}) and propyne (C_3H_4, $\Delta H_f^\circ = 44.3 \pm 0.2$ kJ mol^{-1}) have substantially higher heats of formation than the corresponding alkenes ethylene (C_2H_4, $\Delta H_f^\circ = 12.5 \pm 0.1$ kJ mol^{-1}) and propene (C_3H_6, $\Delta H_f^\circ = 4.6 \pm 0.3$ kJ mol^{-1}).[49] The formation of alkynes from femtosecond laser processing only in the presence of Au NPs suggests that the enhanced plasma energy they provide opens up additional high-energy reaction pathways.

Peaks at m/z 50 and 52 are observed in both the nanosecond and femtosecond samples in Fig. 5. These species are assigned to CH_3Cl with^{35} Cl and^{37} Cl, respectively, in the nanosecond sample because the ratio of the integrated signals of m/z 50/52 is 3.05, closely matching the natural chlorine 35/37 isotopic ratio of 3.12. Moreover, no other alkynes were observed in the nanosecond sample, so the formation of C_4H_2 and C_4H_4 is highly unlikely. In contrast, the m/z 50/52 ratio in the femtosecond sample is 2.14, which indicates that these signals cannot exclusively be attributed to CH_3Cl; instead at least some portion comes from C_4H_2 and C_4H_4, consistent with the observation of other alkynes. We note that the resolution of our MS instrument is not sufficient to resolve the small mass differences between C_4H_2 and CH_3 ^{35}Cl, so it is not possible to definitively conclude that CH_3Cl was formed during femtosecond processing. Nevertheless, the observation of H_2 and reactive chlorine species from femtosecond processing suggest that CH_3Cl can easily be formed under plasma conditions.

CH_3Cl has been observed as a product of photochemical reactions involving Au NPs, $[AuCl_4]^-$, and IPA catalyzed by 488 nm light.[56] The authors proposed that photoexcitation of the surface plasmon resonance (SPR) of the Au NP results in oxidation of IPA to acetone. Subsequent chlorine transfer from $[AuCl_4]^-$ to acetone caused C–C bond cleavage to form CH_3Cl and the acetyl radical, which went on to form acetaldehyde.

18850 | *Phys. Chem. Chem. Phys.*, 2023, **25**, 18844–18853

This journal is © the Owner Societies 2023

This mechanism could also be operative under our nanosecond laser processing conditions because the 532 nm laser wavelength is resonant with the Au NP SPR frequency. Additionally, Cl• radicals formed by homolytic Au–Cl bond cleavage could form CH_3Cl from both IPA and acetone through the reactions

$$Cl^\bullet + (CH_3)_2CHOH \rightarrow CH_3Cl + CH_3CHOH^\bullet \quad (21)$$

$$Cl^\bullet + (CH_3)_2CO \rightarrow CH_3Cl + CH_3CO^\bullet \quad (22)$$

According to the active thermochemical tables (ATcT) database,[57] reaction (21) has $\Delta H^\circ = 12.51 \pm 0.54$ kJ mol^{-1} and reaction (22) is barely endothermic with $\Delta H^\circ = 2.94 \pm 0.4$ kJ mol^{-1}. Because previous gas-phase studies have identified acetone as the major product of Cl• reaction with IPA[58] and the barrier to reaction (22) is lower, it is likely that the CH_3Cl is predominantly formed from reaction of Cl• with acetone. For femtosecond processing, it is also possible that CH_3Cl is formed by direct recombination of Cl• and $CH_3^\bullet$ present in the plasma.

3.4 Discussion

The results from this work both identify a new pathway for two-photon laser reduction of Ag$^+$ by electron-transfer from IPA and reveal more complex reaction pathways involving [AuCl$_4$]$^-$ and Au NPs than observed in previous LRL studies. For the first time, chemical byproducts of laser-induced metal ion reduction in the presence of an organic species have been experimentally characterized. Although previous studies have detected H_2O_2[7,8,10,16,18–20] and H_2[13] as byproducts of femtosecond laser [AuCl$_4$]$^-$ reduction in aqueous solution, the formation of free chlorine species has not previously been observed in any LRL study. Fig. 6 summarizes the reaction pathways of Ag$^+$ (Fig. 6(a)) and [AuCl$_4$]$^-$ (Fig. 6b) observed in our experiments. Detected reaction products and putative intermediate species for each reaction condition (femtosecond or nanosecond laser excitation; water or water/IPA solution) are indicated. In the remainder of this section, we discuss the four main classes of reaction pathways identified in Fig. 6: electron transfer, Au–Cl homolysis, plasma reactions, and Au NP-enhanced IPA decomposition.

Electron transfer from IPA to Ag$^+$ to produce acetone by non-ionizing nanosecond laser excitation presents a new LRL mechanism for Ag$^+$, distinct from previous nanosecond LRL reports in which water ionization reduced Ag$^+$.[21,22] Although photoinduced electron transfer from IPA to Ag$^+$ under UV excitation was proposed decades ago,[33] this work represents the first time that this mechanism was observed using visible light to induce two-photon excitation. It is possible that similar electron transfer mechanisms also operate in the numerous reported Ag NP syntheses using visible light and organic media to reduce Ag$^+$.[5]

The observation of free chlorine from nanosecond LRL of [AuCl$_4$]$^-$ (Fig. 4) provides direct evidence for the Au–Cl homolysis pathways (reactions (3)–(5)) proposed for nanosecond LRL in our previous work.[19] The lack of H_2O_2 formation in nanosecond LRL is also consistent with the observation from X-ray transient absorption spectroscopy that [AuCl$_4$]$^-$ reduction proceeds primarily through these bond homolysis pathways upon UV excitation.[29]
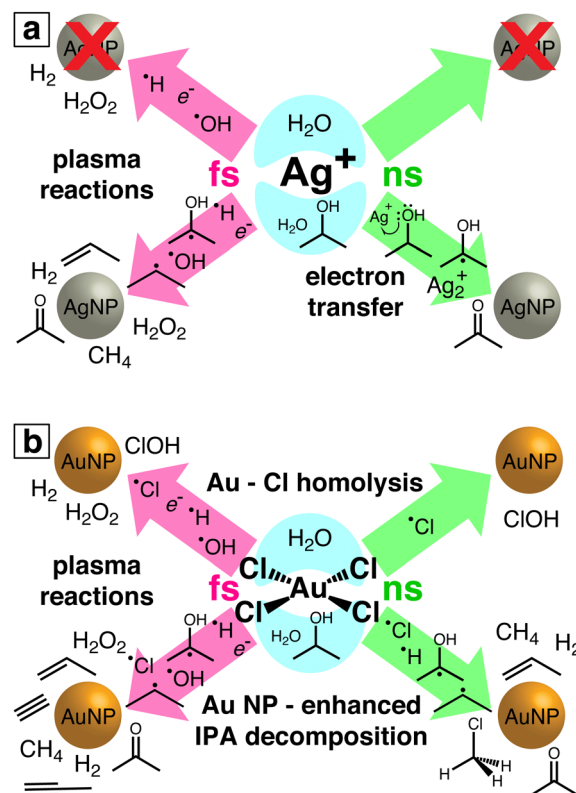

Fig. 6 Schematic of reaction pathways observed in laser-induced reduction of Ag$^+$ (a) and [AuCl$_4$]$^-$ (b). Detected reaction products and putative reaction intermediates are indicated for each reaction condition: femtosecond (pink) or nanosecond (green) laser excitation; water (top) or water/IPA (bottom).

The detection of free chlorine in femtosecond LRL is more surprising because numerous femtosecond LRL studies have established the primacy of plasma reactions (*vide infra*). Moreover, delayed formation of [Au^{2+}Cl$_3$]$^-$ after 800 nm femtosecond excitation observed in X-ray transient absorption spectroscopy confirmed that hydrated electrons initiate [AuCl$_4$]$^-$ reduction.[29] Although a small contribution of direct Au–Cl homolysis in [AuCl$_4$]$^-$ is possible in femtosecond LRL based on the reaction kinetics,[8] it is also possible that the free chlorine species arise by Cl• loss from the clusters [Au$_2$Cl$_2$]$^{2-}$ and [Au$_4$Cl$_4$]$^{4-}$. These clusters were present at times ranging from milliseconds to hundreds of seconds after 800 nm femtosecond laser excitation according to X-ray transient absorption spectroscopy.[29] Excitation of these clusters by a subsequent femtosecond laser pulse could release Cl•. Although the present measurements cannot determine whether free chlorine is released from [AuCl$_4$]$^-$ or small Au^0 clusters, its effects should be taken into account for both nanosecond and femtosecond LRL of other chlorine-containing precursor complexes such as [PtCl$_4$]$^{2-}$ and [PdCl$_4$]$^{2-}$.

Plasma reactions involving e$_{aq}^-$, H•, OH•, and H_2O_2 are well established as the primary reaction pathways that drive femtosecond LRL.[9–11,17–20,24–26] It should be noted that the high-intensity laser excitation can also induce direct Au–Cl homolysis that contributes Cl• to the plasma species present during [AuCl$_4$]$^-$ reduction, as discussed above. Numerous groups have

This journal is © the Owner Societies 2023

Phys. Chem. Chem. Phys., 2023, **25**, 18844–18853 | 18851

demonstrated that the kinetics of metal ion reduction and metal NP sizes can be controlled through addition of chemical scavengers for $e_{aq}{}^{-}$ [11,17,20] and $OH^{\bullet}$.[18,24–26] Although this plasma environment is widely considered to resemble radiolysis conditions,[6,11,17] the present results demonstrate that additional IPA decomposition pathways that form propene are accessible in femtosecond laser plasma that do not occur in radiolysis.[47] This enhanced formation of organic byproducts during femtosecond LRL can affect the metal NP products. No organic ligands were observed on the Au NPs synthesized in water/IPA,[18] but LRL of copper and silver acetylacetonate in IPA produced NPs with a carbon shell.[59,60]

The observed enhanced IPA decomposition when Au NPs are present opens up the possibility of driving the formation of organic products through LRL of $[AuCl_4]^-$, particularly with femtosecond excitation. In particular, our observation of numerous alkynes from IPA decomposition suggests that addition of $[AuCl_4]^-$ or Au NPs may enhance the yields of polyynes (linear chains of sp-hybridized carbons) from femtosecond laser processing of organic liquids. Typically, laser processing of neat organic liquids requires hours to produce observable polyyne yields.[61] Laser ablation of Au in ethanol was found to produce higher yields of polyynes,[62] likely due to Au NP-enhanced plasma reactions. Hence, our results support the potential use of Au NPs to enhance the production of specific organic products by laser processing.

4. Conclusion

Photochemical reaction pathways of Ag^+ and $[AuCl_4]^-$ reduction during nanosecond and femtosecond laser processing in solution were determined using strong-field ionization mass spectrometry and spectroscopic assays. An electron transfer pathway from IPA to Ag^+ induced by two-photon visible excitation with low-fluence nanosecond laser pulses that produces acetone as a byproduct was identified. Free chlorine species were detected after reduction of $[AuCl_4]^-$ by both nanosecond and femtosecond laser pulses, indicating the formation of $Cl^{\bullet}$ as a reaction intermediate. In addition to IPA decomposition pathways observed in radiolysis, femtosecond laser plasma also induces formation of propene, likely due to the actions of laser-induced shock waves. The presence of Au NPs was found to further enhance IPA decomposition, producing alkyne products from femtosecond laser excitation and CH_3Cl from nanosecond laser excitation. Collectively, this knowledge that a plethora of complex reaction pathways occur during LRL of metal precursors can be applied to design laser processing syntheses to better control the properties of metal nanoparticles and enhance yields of organic products.

Author contributions

L. M. Frias Batista: conceptualization, methodology, software, formal analysis, investigation, writing – original draft. M. Moody: methodology, formal analysis, investigation, validation. C. Weththasingha: methodology, formal analysis, investigation, validation. E. Kaplan: methodology, formal analysis, investigation, validation. I. Faruque: formal analysis, investigation, validation. M. S. El-Shall: conceptualization, supervision, resources, funding acquisition, writing - review & editing. K. M. Tibbetts: conceptualization, supervision, resources, funding acquisition, project administration, visualization, writing – review & editing.

Conflicts of interest

There are no conflicts to declare.

Acknowledgements

Notes and references

1 K. Guo, A. Baidak and Z. Yu, *J. Mater. Chem. A*, 2020, **8**, 23029–23058.

2 J. Belloni, M. Mostafavi, H. Remita, J.-L. Marignier and A. Marie-Odile Delcourt, *New J. Chem.*, 1998, **22**, 1239–1255.

3 K. Čubová and V. Čuba, *Radiation Physics and Chemistry*, 2020, **169**, 108774.

4 M. Sakamoto, M. Fujistuka and T. Majima, *J. Photochem. Photobiol., C*, 2009, **10**, 33–56.

5 N. Jara, N. S. Milán, A. Rahman, L. Mouheb, D. C. Boffito, C. Jeffryes and S. A. Dahoumane, *Molecules*, 2021, **26**, 4585.

6 L. M. Frias Batista, A. Nag, V. K. Meader and K. M. Tibbetts, *Sci. China: Phys., Mech. Astron.*, 2022, **65**, 1–45.

7 B. Tangeysh, K. Moore Tibbetts, J. H. Odhner, B. B. Wayland and R. J. Levis, *J. Phys. Chem. C*, 2013, **117**, 18719–18727.

8 K. Moore Tibbetts, B. Tangeysh, J. H. Odhner and R. J. Levis, *J. Phys. Chem. A*, 2016, **120**, 3562–3569.

9 N. Nakashima, K. Yamanaka, M. Saeki, H. Ohba, S. Taniguchi and T. Yatsuhashi, *J. Photochem. Photobiol., A*, 2016, **319–320**, 70–77.

10 V. K. Meader, M. G. John, C. J. Rodrigues and K. M. Tibbetts, *J. Phys. Chem. A*, 2017, **121**, 6742–6754.

11 H. Belmouaddine, M. Shi, P.-L. Karsenti, R. Meesat, L. Sanche and D. Houde, *Phys. Chem. Chem. Phys.*, 2017, **19**, 7897–7909.

12 C. Zhao, S. Qu, J. Qiu and C. Zhu, *J. Mater. Res.*, 2003, **18**, 1710–1714.

13 T. Nakamura, Y. Mochidzuki and S. Sato, *J. Mater. Res.*, 2008, **23**, 968–974.

14 T. Nakamura, Y. Herbani, D. Ursescu, R. Banici, R. V. Dabu and S. Sato, *AIP Adv.*, 2013, **3**, 082101.

15 Muttaqin, T. Nakamura and S. Sato, *Appl. Phys. A: Mater. Sci. Process.*, 2015, **120**, 881–888.

16 J. H. Odhner, K. Moore Tibbetts, B. Tangeysh, B. B. Wayland and R. J. Levis, *J. Phys. Chem. C*, 2014, **118**, 23986–23995.

17 H. Belmouaddine, M. Shi, L. Sanche and D. Houde, *Phys. Chem. Chem. Phys.*, 2018, **20**, 23403–23413.

18852 | *Phys. Chem. Chem. Phys.*, 2023, **25**, 18844–18853

This journal is © the Owner Societies 2023

18 L. M. Frias Batista, V. K. Meader, K. Romero, K. Kunzler, F. Kabir, A. Bullock and K. M. Tibbetts, *J. Phys. Chem. B*, 2019, **123**, 7204–7213.

19 C. J. Rodrigues, J. A. Bobb, M. G. John, S. P. Fisenko, M. S. El-Shall and K. M. Tibbetts, *Phys. Chem. Chem. Phys.*, 2018, **20**, 28465–28475.

20 K. Y. Putri, A. L. Fadli, F. A. Umaroh, Y. Herbani, C. Imawan and D. Djuhana, *Radiat. Phys. Chem.*, 2022, **199**, 110269.

21 J. P. Abid, A. W. Wark, P. F. Brevet and H. H. Girault, *Chem. Commun.*, 2002, 792–793.

22 U. Y. Qazi, S. Kajimoto and H. Fukumura, *Chem. Lett.*, 2014, **43**, 1693–1695.

23 T. Nakamura, H. Magara, Y. Herbani and S. Sato, *Appl. Phys. A: Mater. Sci. Process.*, 2011, **104**, 1021.

24 V. K. Meader, M. G. John, L. M. Frias Batista, S. Ahsan and K. M. Tibbetts, *Molecules*, 2018, **23**, 532.

25 Y. Herbani, T. Nakamura and S. Sato, *J. Phys. Conf. Ser.*, 2017, **817**, 012048.

26 C. M. Nguyen, L. M. Frias Batista, M. G. John, C. J. Rodrigues and K. M. Tibbetts, *J. Phys. Chem. B*, 2021, **125**, 907–917.

27 S. Eustis, H.-Y. Hsu and M. A. El-Sayed, *J. Phys. Chem. B*, 2005, **109**, 4811–4815.

28 M. Harada and S. Kizaki, *Cryst. Growth Des.*, 2016, **16**, 1200–1212.

29 X. Liu, X. Zhang, D. Khakhulin, P. Su, M. Wulff, F. Baudelet, T.-C. Weng, Q. Kong and Y. Sun, *J. Phys. Chem. Lett.*, 2022, **13**, 8921–8927.

30 P. Vanýsek, *CRC Handbook of Chemistry and Physics*, CRC Press, Boca Raton, FL, 1998, ch. Electrochemical Series.

31 D. Spadaro, E. Barletta, F. Barreca, G. Currò and F. Neri, *Appl. Surf. Sci.*, 2010, **256**, 3812–3816.

32 L. Maretti, P. S. Billone, Y. Liu and J. C. Scaiano, *J. Am. Chem. Soc.*, 2009, **131**, 13972–13980.

33 H. Hada, Y. Yonezawa, A. Yoshida and A. Kurakake, *J. Phys. Chem.*, 1976, **80**, 2728–2731.

34 A. Henglein, *Ber. Bunsenges. Phys. Chem.*, 1977, **81**, 556–561.

35 R. Tausch-Treml, A. Henglein and J. Lilie, *Ber. Bunsenges. Phys. Chem.*, 1978, **82**, 1335–1343.

36 G. L. Gutsev, D. Ampadu Boateng, P. Jena and K. M. Tibbetts, *J. Phys. Chem. A*, 2017, **121**, 8414–8424.

37 E. V. Barmina, A. V. Simakin and G. A. Shafeev, *Chem. Phys. Lett.*, 2017, **678**, 192–195.

38 A. V. Simakin, M. E. Astashev, I. V. Baimler, O. V. Uvarov, V. V. Voronov, M. V. Vedunova, M. A. Sevost'yanov, K. N. Belosludtsev and S. V. Gudkov, *J. Phys. Chem. B*, 2019, **123**, 1869–1880.

39 M. R. Kalus, N. Bärsch, R. Streubel, E. Gökce, S. Barcikowski and B. Gökce, *Phys. Chem. Chem. Phys.*, 2017, **19**, 7112–7123.

40 M.-R. Kalus, R. Lanyumba, N. Lorenzo-Parodi, M. A. Jochmann, K. Kerpen, U. Hagemann, T. C. Schmidt, S. Barcikowski and B. Gökce, *Phys. Chem. Chem. Phys.*, 2019, **21**, 18636–18651.

41 C. Aeppli, M. Berg, T. B. Hofstetter, R. Kipfer and R. P. Schwarzenbach, *J. Chromatogr. A*, 2008, **1181**, 116–124.

42 D. Harp and C. C. Hach, *Current Technology of Chlorine Analysis for Water and Wastewater*, Hach Company, Loveland, CO, USA, 2003.

43 G. Eisenberg, *Ind. Eng. Chem., Anal. Ed.*, 1943, **15**, 327–328.

44 G. Maatz, A. Heisterkamp, H. Lubatschowski, S. Barcikowski, C. Fallnich, H. Welling and W. Ertmer, *J. Opt. A*, 1999, **2**, 59–64.

45 H. Kierzkowska-Pawlak, J. Tyczkowski, A. Jarota and H. Abramczyk, *Appl. Energy*, 2019, **247**, 24–31.

46 https://webbook.nist.gov/chemistry/. Last checked 1/17/22.

47 L. Gilles and J. Sutton, *J. Chim. Phys.*, 1970, **67**, 128–138.

48 C. Von Sonntag and H.-P. Schuchmann, *Photolysis of Saturated Alcohols, Ethers, and Amines*, John Wiley & Sons, Ltd, 1977, pp. 59–145.

49 C. F. Goldsmith, G. R. Magoon and W. H. Green, *J. Phys. Chem. A*, 2012, **116**, 9033–9057.

50 G. E. Adams and R. L. Willson, *Trans. Faraday Soc.*, 1969, **65**, 2981–2987.

51 D. C. Guerin, R. F. Fernsler and V. A. Shamamian, *J. Vac. Sci. Technol., A*, 2003, **21**, 1724–1733.

52 T. Juhasz, G. A. Kastis, C. Suárez, Z. Bor and W. E. Bron, *Lasers Surg. Med.*, 1996, **19**, 23–31.

53 W. Ishikawa and S. Sato, *Chem. Phys. Chem.*, 2020, **21**, 2104–2111.

54 W. Liu, S. A. Andrews, M. I. Stefan and J. R. Bolton, *Water Res.*, 2003, **37**, 3697–3703.

55 R. Lachaine, É. Boulais and M. Meunier, *ACS Photonics*, 2014, **1**, 331–336.

56 V. Mohan, E. Wu, J. Heo, A. Das and P. K. Jain, *ACS Energy Lett.*, 2021, **6**, 1980–1989.

57 B. Ruscic and D. H. Bross, Active Thermochemical Tables (ATcT) values based on ver. 1.124 of the Thermochemical Network, Argonne National Laboratory, Lemont, Illinois 2022, https://atct.anl.gov/Thermochemical.

58 T. Yamanaka, M. Kawasaki, M. D. Hurley, T. J. Wallington, W. F. Schneider and J. Bruce, *Phys. Chem. Chem. Phys.*, 2007, **9**, 4211–4217.

59 A. Nag, L. M. Frias Batista and K. M. Tibbetts, *Nanomaterials*, 2021, **11**, 814.

60 A. Nag, C. M. Nguyen and K. M. Tibbetts, *Appl. Surf. Sci.*, 2023, **610**, 155384.

61 A. Ramadhan, M. Wesolowski, T. Wakabayashi, H. Shiromaru, T. Fujino, T. Kodama, W. Duley and J. Sanderson, *Carbon*, 2017, **118**, 680–685.

62 B. Pan, J. Xiao, J. Li, P. Liu, C. Wang and G. Yang, *Sci. Adv.*, 2015, **1**, e1500857.

This journal is © the Owner Societies 2023

Phys. Chem. Chem. Phys., 2023, **25**, 18844–18853 | 18853